HHS Public Access

Author manuscript

Stroke. Author manuscript; available in PMC 2023 February 01.

Published in final edited form as:

Stroke. 2022 February ; 53(2): 595–604. doi:10.1161/STROKEAHA.121.035638.

Imaging high-risk atherothrombosis using a novel fibrin-binding positron emission tomography probe

David Izquierdo-Garcia, PhD[1,2], **Himashinie Diyabalanage, PhD**[3], **Ian A. Ramsay, BS**[1,3,4], **Nicholas J. Rotile, BA**[1,4], **Adam Mauskapf, BS**[5], **Ji-Kyung Choi, PhD**[1], **Thomas Witzel, PhD**[1], **Valerie Humblet, PhD**[3], **Farouc A. Jaffer, MD PhD**[5], **Anna-Liisa Brownell, PhD**[6], **Ahmed Tawakol, MD**[7], **Ciprian Catana, MD PhD**[1,4], **Mark F. Conrad, MD**[8], **Peter Caravan, PhD**[1,4,*], **Ilknur Ay, MD PhD**[1,*]

[1]Athinoula A. Martinos Center for Biomedical Imaging, Department of Radiology, Massachusetts General Hospital and Harvard Medical School, Charlestown, MA

[2]Harvard-MIT Department of Health Sciences and Technology, Massachusetts Institute of Technology, Cambridge, MA

[3]Collagen Medical, LLC, Belmont, MA

[4]The Institute for Innovation in Imaging, Department of Radiology, Massachusetts General Hospital, Charlestown, MA

[5]Cardiovascular Research Center, Division of Cardiology, Department of Medicine Massachusetts General Hospital and Harvard Medical School, Boston, MA

[6]Gordon Center for Medical Imaging, Department of Radiology, Massachusetts General Hospital and Harvard Medical School, Charlestown, MA

[7]Nuclear Cardiology, Division of Cardiology, Department of Medicine, Massachusetts General Hospital and Harvard Medical School, Boston, MA

[8]Division of Vascular and Endovascular Surgery, Massachusetts General Hospital and Harvard Medical School, Boston, MA

Abstract

Background and Purpose: High-risk atherosclerosis is an underlying etiology in cardiovascular events, yet identifying the specific patient population at immediate risk is still challenging. Here, we used a rabbit model of atherosclerotic plaque rupture and human carotid endarterectomy specimens to describe the potential of molecular fibrin imaging as a tool to identify thrombotic plaques.

Correspondence: Ilknur Ay, MD, PhD, Building 149, Room 2301, 13th Street, Charlestown, MA 02129, Phone: 617-643-0193, FAX: 617-726-7422, iay@mgh.harvard.edu.

*Authors contributed equally

List of the Supplemental Materials with a callout to any references that are in the Supplemental Material only:
Supplemental Material
Online Table I
Online Figures I–VIII
Reference 54

Methods: Atherosclerotic plaques in rabbits were induced using a high-cholesterol diet and aortic balloon injury (N=13). Pharmacological triggering was used in a group of rabbits (n=9) to induce plaque disruption. Animals were grouped into thrombotic and non-thrombotic plaque groups based on gross pathology (gold standard). All animals were injected with a novel fibrin-specific probe ^{68}Ga-CM246 followed by PET/MR imaging 90 minutes later. ^{68}Ga-CM246 was quantified on the PET images using tissue-to-background (back muscle) ratios (TBR) and standardized uptake value (SUV).

Results: Both TBR and SUV were significantly higher in the thrombotic vs. non-thrombotic group ($p<0.05$). Ex vivo PET and autoradiography of the abdominal aorta correlated positively with in vivo PET measurements. Plaque disruption identified by ^{68}Ga-CM246 PET agreed with gross pathology assessment (85%). In ex vivo surgical specimens obtained from patients undergoing elective carotid endarterectomy (N=12), ^{68}Ga-CM246 showed significantly higher binding to carotid plaques compared to a D-cysteine non-binding control probe.

Conclusions: We demonstrated that molecular fibrin PET imaging using ^{68}Ga-CM246 could be a useful tool to diagnose experimental and clinical atherothrombosis. Based on our initial results using human carotid plaque specimens, in vivo molecular imaging studies are warranted to test ^{68}Ga-CM246 PET as a tool to stratify risk in atherosclerotic patients.

Introduction

Atherosclerotic lesions at bifurcations and curves of large arteries of the brain are a prominent cause of stroke[1]. Approximately one out of every five strokes are caused by atherosclerotic plaques in the cerebral circulation[2]. Seventy-five percent of atherosclerotic plaques are seated at the bifurcation of the extracranial common carotid artery, marking carotid atherosclerosis as one of the leading causes of stroke, along with atrial fibrillation[3]. Carotid plaques can lead to stroke by means of flow-limiting arterial stenoses or occlusion (hemodynamic stroke) and artery to artery thromboembolism[4]. Embolic fragments that arise from thrombotic material overlying a ruptured, eroded, or ulcerated plaque are responsible for up to 90% of strokes associated with carotid atherosclerosis[3]. Concerningly, existing risk stratification tools based on the degree of stenosis provided a prediction of only moderate discriminative power[5,6]. In the NASCET trial of symptomatic carotid stenosis, 86% of study subjects with moderate to severe stenosis did not develop a stroke during the one-year follow-up period, showing that the degree of carotid stenosis by itself has a limited ability for risk prediction and could result in unnecessary revascularization procedures that carry risk[6]. The problem is even more acute in asymptomatic carotid stenosis, where the annual ipsilateral stroke rate in patients with stenosis ≥50% hovers around only 0.5% to 1.0%[7,8]. Better approaches to identify patients at risk of developing a stroke and, hence, the likelihood of benefit from carotid revascularization are needed.

The current state of the art used in carotid artery imaging includes an ultrasound (US), CT, and MR[9]. Duplex US is the standard imaging modality for carotid plaques[10]. Still, each of these methods has suboptimal sensitivity and specificity in identifying many features of vulnerable plaque[8]. The intravascular US can provide more information on plaque structure[11]. Still, it is an invasive procedure that carries a risk to the patient and is infrequently performed in the carotid artery. CT is accepted as a reliable tool to

image carotid plaque and its components, but detecting fibrous cap status and intraplaque hemorrhage is difficult[9]. Also, CT carries the risk due to contrast material (i.e., anaphylactic reaction and nephropathy) and radiation. MR imaging can help identify plaque components, including fibrous cap and intraplaque hemorrhage[12], but does not specifically image fibrin. For a subgroup of patients, gadolinium toxicity may confer risk for contrast MR imaging, which in some cases could outweigh the radiation hazard[9]. Another limitation of US, CT, and MRI is that they provide information on only the plaque's anatomical characteristics rather than the pathophysiological events happening at the molecular level. Moreover, these three standard imaging methods are efficient only in advanced-stage atherosclerotic disease[13]. Molecular PET imaging offers a high-sensitivity solution to these limitations through probes that detect molecules involved in the pathophysiological process leading to thromboembolism.

Thrombus is present in carotid plaques in 74% of ischemic stroke patients that underwent endarterectomy[14]. The majority of these cases (90%) arise from plaque rupture, while the remaining 10% have thrombus associated with plaque erosion[14]. Furthermore, carotid plaques obtained from patients after the initial cerebrovascular event continue to have thrombus associated with them, suggesting increased susceptibility to secondary events[14]. We hypothesize that thrombus imaging using a fibrin-specific molecular probe could identify plaques with recent rupture/hemorrhage events and better stratify patients for revascularization. Here, we report the feasibility of the fibrin-specific probe ^{68}Ga-CM246 to detect atherosclerotic plaque rupture in a rabbit model using PET/MR imaging. We also report the efficacy of ^{68}Ga-CM246 in specimens obtained from patients who underwent carotid endarterectomy surgery.

Methods

The data that support the findings of this study are available from the corresponding author upon reasonable request. All experiments were approved by the Institutional Animal Care and Use Committee at Massachusetts General Hospital (2016N000154) and the Institutional Review Board at Massachusetts General Hospital (2016P001353). Animals were randomized into plaque rupture or control groups. PET/MRI data were analyzed by a blinded expert (Dr. Izquierdo-Garcia).

Fibrin-specific probe 68Ga-CM246 was synthesized, and its pharmacokinetics were tested in healthy rabbits, as detailed in Supplemental Material.

Rabbit model of plaque rupture

Atherosclerosis and subsequent plaque disruption were induced in thirteen adult male and female New Zealand white rabbits, as reported previously[15]. Atherosclerotic plaque formation was generated by balloon injury of the abdominal aorta in rabbits fed with high cholesterol diet. Animals allocated to the plaque rupture group (n=9) were injected with Russell's viper venom (0.15 mg/kg, IP; Sigma-Aldrich) and histamine (0.02 mg/kg; IV; Sigma-Aldrich), whereas control rabbits (n=4) received no injection. About one hour after the last injection, animals were placed in a combined BrainPET–3T MR system (Siemens Healthineers, Erlangen, Germany) for simultaneous PET/MR imaging. All rabbits were

injected with ^{68}Ga-CM246 (2.4 – 5.6 MBq/kg; IV). PET images were reconstructed using a 3D OP-OSEM algorithm with 6-iterations, and 16 subsets from the emission data collected 90–105 min post-injection (p.i.). During PET acquisition, the following MR data were acquired simultaneously using an in-house built surface coil in conjunction with a birdcage 8-channel head coil (Siemens Healthineers): a magnetization prepared rapid-gradient echo (MPRAGE), a dark-blood T2 sequence, and a time-of-flight (ToF) sequence. Immediately after in vivo imaging, animals were euthanized. The abdominal aorta, the inferior vena cava, and the right common carotid artery were harvested to confirm the quantification accuracy of in vivo PET[16]. For this, tissues were tested using ex vivo PET imaging (20 min acquisition) and autoradiography. Then, the abdominal aorta was cut into four equal-length segments and fixed using 4% paraformaldehyde. Each segment's rostral part was used for histology (Carstairs' staining). The remaining segments were cut open for gross pathology to detect thrombus formation in the lumen. Thrombus area was calculated from the digital images using Image J by measuring the area of the thrombus and the total luminal vessel area and expressed as % of the total luminal surface area. See Supplemental Material for details.

Ex vivo studies of human carotid endarterectomy specimens

We obtained 12 fresh, discarded surgical specimens from asymptomatic patients who underwent elective carotid endarterectomy at Massachusetts General Hospital. Specimens were processed for histology (Carstairs' staining), autoradiography, and probe binding assay. For autoradiography, sections were incubated with ^{68}Ga-CM246 or D-cysteine non-binding control probe ^{68}Ga-CM249 for 45 minutes. Autoradiography was performed after three washes of PBS. The exposure time was 2 minutes. The probe binding assay involved incubating ^{68}Ga-CM246 or ^{68}Ga-CM249 with about 10 mg of plaque sample for 45 minutes and measuring the activity bound to the plaque tissue after two wash cycles. See Supplemental Material for details.

Data analysis

The MR images were used to define the abdominal aorta from the renal to the iliac bifurcation semi-automatically and divided into four equal length segments (~2 cm each). Background regions of interest (ROIs) were placed on the back muscle. The corresponding ROIs were copied to the PET images, and the mean and maximum standardized uptake values (SUV and SUV_{max}, respectively)[17] and aorta tissue-to-background muscle ratios (TBR) and maximum TBR (TBR_{max}) were calculated. Data are reported *per-segment* and *per-animal*, where ROI values across all four segments were averaged. Gross pathology, scored as thrombus-negative or thrombus-positive, defined the gold standard of plaque thrombosis. Receiver operating characteristic (ROC) curves were used to characterize the diagnostic efficacy of ^{68}Ga-CM246 PET. In human specimens, the fibrin-positive area was determined in Carstairs'-stained sections using the Image J software and expressed as a percentage of the total section area. In sections where the plaque occupied more than 180° of the vessel wall, the most-positive half (% fibrin) was used, as reported before for CD68 staining[18]. See Supplemental Material for details.

Statistical analysis

Data were expressed as mean ± SEM. The normality of data was analyzed using the Kolmogorov-Smirnov test (GraphPad Prism 8.3). Differences between groups were compared using linear models (see Supplemental Material for details). Correlation plots and correlation values (Pearson's for the normally distributed data and Spearman's for the non-normally distributed) were calculated among the in vivo, ex vivo, autoradiography, and histology measurements. A P value <0.05 was considered statistically significant.

Results

^{68}Ga-CM246 pharmacokinetics and rabbit model of plaque rupture

^{68}Ga-CM246 has favorable pharmacokinetics in healthy rabbits, with a blood half-life of 23 min, and is functionally intact and not metabolized after injection (see Supplemental Material, Sup. Fig. I – V). None of the control (N=4, non-triggered) rabbits demonstrated plaque disruption. The success of the model to induce plaque thrombosis, as determined by gross pathology, was 77% (n=7/9). Therefore the plaque thrombosis group comprised n=7 animals, and the non-plaque thrombosis group comprised n=6 animals. Similarly, by segment (Fig. 1A), there were n=22 ruptured vs. n=30 unruptured segments. Rabbits with successful triggering of plaque thrombosis had intraluminal thrombi attached to the vessel wall (Fig. 1B; thrombus area: 6.87 ± 0.96 % of the total luminal surface area, n=7), whereas the aortic lumina of the control rabbits were clear (Fig. 1C). Carstairs' staining corroborated gross pathology results by displaying fibrin-specific bright red staining in the area of disrupted plaques in rabbits with intraluminal thrombus (Fig. 1D–E).

Pilot dynamic imaging indicated that plaque uptake and TBR remained similar at 90–105 minutes p.i. Thus, this time point was chosen for data collection/analysis (see Sup. Fig. VI for details) in all animals, but one (for which imaging was acquired up to 80 min).

^{68}Ga-CM246 PET/MRI and ex vivo studies

In vivo PET/MR images of rabbits without thrombosis (Fig. 2A–C) showed lower ^{68}Ga-CM246 uptake along the abdominal aorta compared with rabbits with plaque disruption (Fig. 2D–F). Group analysis (Fig. 3A–B) showed that probe uptake in the abdominal aorta was higher in segments with plaque disruption vs. undisrupted segments for TBR (8.42 ± 0.51 vs. 6.32 ± 0.38, p<0.05), TBR_{max} (9.75 ± 0.61 vs. 7.44 ± 0.43, p<0.05), SUV (0.95 ± 0.14 vs. 0.65 ± 0.08, p<0.05), and SUV_{max} (1.08 ± 0.15 vs. 0.73 ± 0.09, p<0.05). Per-animal analysis (Sup. Fig. VII) showed similar results as the per-segment analysis. Inclusion/exclusion of non-ruptured animals within the control group offered the same results (Supplemental Material).

ROC analysis was used to measure diagnostic accuracy and identify the best thresholds to define plaque disruption by in vivo PET imaging. TBR_{max} was the most accurate with 100% sensitivity and 85% accuracy (only two false positives), Table 1.

There was a strong significant correlation between in vivo PET results and ex vivo PET images and autoradiography (r=0.91 and r=0.74, respectively, Fig 3C–D). Ex vivo PET

images and autoradiography showed similar segmental differences in focal uptake as the in vivo PET images (Fig. 4 and Supplemental Material).

Ex vivo studies of human carotid endarterectomy specimens

The binding of ^{68}Ga-CM246 and control probe ^{68}Ga-CM249 to human carotid plaques assessed by autoradiography (Fig.5A–B, E) and by a tissue binding assay (Fig. 5F) showed significantly higher uptake of ^{68}Ga-CM246 compared to ^{68}Ga-CM249 ($P<0.05$ for both). However, there was substantial interpatient variability in ^{68}Ga-CM246 uptake in both experiments (Fig. 5E–F). Assuming the ^{68}Ga-CM249 result represents a non-specific binding, we calculated the average ^{68}Ga-CM249 value for all plaques and average plus 1 or 2 standard deviations (SD) as dashed lines in Fig. 5E–F. This analysis stratified the plaque specimens in terms of being fibrin rich or fibrin poor. Carstairs' staining results were congruent with the autoradiography and tissue binding assay results. In some specimens, high ^{68}Ga-CM246 uptake and substantial fibrin presence were detected (Fig. 5A–D), whereas low-uptake specimens had comparatively less fibrin (Sup. Fig. VIII). Uptake of ^{68}Ga-CM246, as determined by autoradiography, and the specimen fibrin content, as detected by Carstairs' staining, correlated significantly ($R^2 = 0.54$, $p<0.05$).

Discussion

This study aimed to provide a better tool for risk stratification of carotid disease based on in vivo imaging of fibrin-rich thrombus using a novel PET tracer ^{68}Ga-CM246. In carotid atherosclerosis, stroke risk stratification currently relies on the degree of stenosis and symptoms. Revascularization surgery is considered in patients having stenosis over 50% (if symptomatic) and 60% (if asymptomatic)[19]. However, multicenter trials show that this approach has a limited risk prediction ability, potentially resulting in unnecessary revascularization operations[6]. Identifying additional high-risk plaque characteristics could enhance stenosis-based risk stratification approaches. Based on morphological markers like plaque volume, size of the lipid-rich necrotic core, fibrous cap thickness, and intraplaque hemorrhage, a vulnerable carotid plaque has been described[20]. Anatomical imaging, including US, CT, and MRI, helps determine the plaque morphology and check for vulnerability signs. The advantages and disadvantages of these modalities on carotid plaque imaging are well documented though there is a lack of studies directly comparing them[21]. Overall, MRI is accepted superior to other techniques due to its high sensitivity and specificity for plaque components and reproducibility of the results[22,23]. There is, however, a consensus that none of the current imaging techniques is reliable by itself to identify the high-risk carotid plaque[24]. Molecular imaging provides additional information on standard anatomical imaging by visualizing the pathophysiological process within the plaque. Earlier studies in animals, particularly in ApoE$^{-/-}$ mice, demonstrated the feasibility of in vivo molecular imaging of plaque macrophages, activated endothelial cells, inflammatory proteases, and apoptosis and helped our understanding of the pathophysiology of the disease[25]. Some of these molecular imaging probes were tested in patients undergoing carotid endarterectomy. Among these, ultrasmall-superparamagnetic-iron-oxide (USPIO) particles (to image plaque macrophages in T2*-weighted MRI)[26], ^{111}In-platelet scintigraphy[27], ^{18}F-sodium fluoride (to image microcalcifications by PET)[28], ^{18}F-FDG

(to image inflammatory cell activity by PET)[29,18], and annexin A5 (to image apoptosis by SPECT)[30] yielded encouraging results to detect carotid plaques. However, except for ^{18}F-FDG and ^{18}F-sodium fluoride, these probes did not become clinically standard either due to pharmacokinetic or feasibility issues or lack of clear clinical utility. ^{18}F-FDG PET imaging is highly reproducible but suffers from low specificity (e.g., metabolically active nearby tissues like lymph nodes may result in artifacts)[17,31]. Its signal is also confounded by high blood glucose, and its pharmacokinetics is altered in patients with decreased renal function[32]. Nevertheless, a recent multicenter prospective study suggests that increased ^{18}F-FDG uptake could provide additional information over what is provided by the degree of stenosis alone for recurrent stroke in patients with recently symptomatic moderate to severe carotid stenosis[33,34]. In the causal chain of events that starts from plaque formation to plaque rupture with subsequent stroke, plaque inflammation is an intermediate process, while plaque thrombosis is a more downstream biological step, closer to plaque rupture. Further details about the advantages and disadvantages of the current imaging methods targeting atherosclerosis can be found in great detail in focused reviews[35,36].

Activated platelets, glycoprotein IIb/IIIa, tissue factor, and fibrin are suggested as target molecules for thrombus imaging[37]. Among these, fibrin presents itself as a unique candidate since it is only present in the thrombus, offering greater signal-to-noise advantages[38]. Small fibrin-specific peptides were identified by phage display, further optimized, and derivatized with imaging reporters to create optical, MR, or nuclear imaging probes[39–42]. Fibrin-binding MR probes, EP-1873, and its pharmacokinetically improved version, EP-2104R, were used successfully in animal models and patients with thrombus[38,40,43]. Given the low sensitivity of molecular MRI and the required waiting time between pre-and post-injection scans, PET versions of these probes were developed. Efficacy of ^{64}Cu-labelled fibrin binding probes was demonstrated in animal models of thrombosis and thrombolysis and patients with left atrial appendage thrombus[43–46]. Here, we developed and tested a ^{68}Ga-labelled version of a fibrin-binding peptide. Given the compact and user-friendly nature of gallium generators in contrast to high-energy cyclotrons required to produce ^{64}Cu, the ^{68}Ga-CM246 probe can be made cost-effectively at the imaging facility's site.

Our overall hypothesis is that fibrin-rich thrombus demarcates high-risk carotid plaques for both asymptomatic and symptomatic patients. As a prelude to testing this hypothesis in prospective clinical trials, here we show that the fibrin-binding probe ^{68}Ga-CM246 detects thrombus non-invasively in a rabbit model of atherothrombosis and binds fibrin in human carotid plaques. Based on the results presented here, ^{68}Ga-CM246 imaging can be developed as a valuable tool to add to the plaque risk stratification workup, either alone or with other molecular imaging markers.

Our results show that ^{68}Ga-CM246 is specific for fibrin, and it has excellent pharmacokinetic properties, including rapid uptake into the thrombus, fast blood background clearance, and no evidence of metabolism as assessed by HPLC analysis. The rapid clearance of ^{68}Ga-CM246 has an advantage over other thrombus imaging approaches based on fibrin-based antibodies or antibody fragments where long circulation times require delayed imaging[47–49]. In vivo PET results demonstrated that atherosclerotic plaque disruption in rabbits could be detected and quantified using ^{68}Ga-CM246 PET/MR imaging.

The best imaging time for the acquisition was ~ 90 to 105 min p.i., a suitable timing for a clinically translatable tracer. There was a considerable agreement (85%) between in vivo PET and gross pathology. It is worth noting that similar results were achieved independent of the analysis approach (i.e., per-segment or per-animal). Thus, in vivo ^{68}Ga-CM246 imaging has the potential to detect thrombi in human carotid plaques (size of which are similar to the segments analyzed here) as well as larger arterial pathologies like aortic aneurysm[50].

In our study, ex vivo human carotid endarterectomy data indicate that subclinical fibrin/thrombus is present in these patients in varying degrees. Although our limited sample size did not allow us to stratify the data based on fibrin content and ^{68}Ga-CM246 binding, we could discern two main groups: plaques with high-fibrin content and low-fibrin content. Not surprisingly, ^{68}Ga-CM246 uptake into the carotid plaques was in accordance with fibrin availability in the tissue, as detected by Carstairs' staining. Overall, our results corroborate that: a) ^{68}Ga-CM246 can detect fibrin in vivo / ex vivo in human carotid plaques, and b) that there is likely a range of probe uptake values in patients with carotid plaques depending on the degree of fibrin deposition. Therefore, our next step would be to study carotid atherosclerosis patients and analyze the degree of ^{68}Ga-CM246 fibrin uptake and the development of symptoms over time.

This study has some limitations, including technical challenges related to PET imaging of the abdominal aorta. During PET imaging, partial volume effect (PVE) degrades the PET signal by spilling the signal to/from adjacent tissues[51]. Correcting for PVE requires accurate registration between the PET and MR images, excellent delineation of the ROIs, and homogeneous uptake in every ROI[17]. ROI size needs to be small enough to keep them homogenous and large enough to minimize noise due to motion artifacts like breathing[51]. Additionally, plaque disruption is likely focally localized, resulting in considerable heterogeneity around the ROIs chosen in this study. Moreover, only a couple of animals showed increased uptake near the ROIs around the aorta, while the rest had no significant uptake nearby. Lastly, in vivo PET imaging and histopathology co-localization was technically challenging and might contribute to some degree of data inconsistency. In addition, the animal model used in this study is not an ideal model to mimic human carotid disease that has a preference for bifurcations and curvatures, there are suitable mouse models for that[52,53]. However, rabbit model allows imaging with spatial resolution comparable to clinical settings whereas mouse models do not. Lastly, even though we propose to develop fibrin imaging in patients with carotid plaque as a tool to identify those at risk for stroke, this imaging modality would not be expected to predict stroke risk due to hemodynamic compromise.

In summary, we have shown here that in vivo imaging of plaque disruption is feasible using ^{68}Ga-CM246 with PET/MRI. It is highly sensitive and specific compared to the gold standard of gross pathology that ^{68}Ga-CM246 detects heterogeneous fibrin presence in asymptomatic human carotid plaque specimens. Therefore, we foresee a future for ^{68}Ga-CM246 PET/MR imaging as a potentially clinically valuable tool in carotid atherosclerosis patients whose characterization of the lesion would affect the case management. As a next

step, we plan to prospectively test our probe in patients with a carotid plaque and compare the predictive values of different imaging modalities.

Supplementary Material

Refer to Web version on PubMed Central for supplementary material.

Acknowledgments

Funding Sources:

This study was supported by NIH/NHLBI HHSN268201400044C SBIR Topic 85, Phase II, Development of Molecular Imaging Agents and Methods to Detect High Risk Atherosclerotic Plaques to Collagen Medical / Subcontract to MGH. Additional support from the NHLBI, R01HL122388 and R01HL150538 (to FAJ) and R01HL109448 (to PC), as well as the NIH Office of the Director, S10OD010650 and S10OD025234 (to PC) is acknowledged. This research was carried out in whole at the Athinoula A. Martinos Center for Biomedical Imaging at the Massachusetts General Hospital, using resources provided by the Center for Functional Neuroimaging Technologies, P41RR14075, a P41 Regional Resource supported by the Biomedical Technology Program of the National Center for Research Resources (NCRR), National Institutes of Health.

Disclosures:

Peter Caravan has equity in and is a consultant to Collagen Medical, LLC, the company holding the patent rights to the peptide used in this work. Dr. Caravan's interests were reviewed and are managed by Massachusetts General Hospital and Mass General Brigham in accordance with their conflict of interest policies. Valerie Humblet is an employee of Collagen Medical. Farouc A. Jaffer reports compensation from Magenta Medical for consultant services; grants from Siemens Medical Solutions USA, Inc.; grants from Teleflex Medical Incorporated; compensation from BIOTRONIK INC. for other services; a patent issued for Intravascular Imaging licensed to Canon U.S.A., Inc.; grants from Boston Scientific Corporation; compensation from ASAHI INTECC USA, INC. for other services; stock options in DurVena; a patent issued for Intravascular imaging licensed to Spectrawave; compensation from BIOTRONIK INC. for consultant services; compensation from Boston Scientific Corporation for consultant services; stock holdings in Intravascular Imaging Inc.; grants from Siemens Medical Solutions USA, Inc.; grants from Canon U.S.A., Inc.; a patent issued for Intravascular imaging licensed to Terumo BCT, Inc.; grants from ShockWave Medical, Inc; and compensation from IMDS for other services. Ahmed Tawakol reports grants from Genentech; compensation from Actelion Pharmaceuticals for consultant services; and compensation from Esperion for consultant services.

Non-standard Abbreviations and Acronyms

SUV/SUVmax	Standardized uptake value/maximum standardized uptake value
TBR, TBRmax	Tissue-to-background ratios/maximum tissue-to-background ratios
US	Ultrasound
p.i.	post injection
ToF	Time of Flight
ROIs	Regions of Interest
PVE	Partial Volume Effect
AA	Abdominal aorta
IVC	Inferior vena cava

CA	Carotid artery

References

1. Hademenos GJ, Massoud TF. Biophysical mechanisms of stroke. Stroke. 1997;28:2067–2077. doi: 10.1161/01.str.28.10.2067 [PubMed: 9341720]
2. Benjamin EJ, Muntner P, Alonso A, Bittencourt MS, Callaway CW, Carson AP, Chamberlain AM, Chang AR, Cheng S, Das SR, et al. Heart Disease and Stroke Statistics-2019 Update: A Report From the American Heart Association. Circulation. 2019;139:e56–e528. doi: 10.1161/CIR.0000000000000659 [PubMed: 30700139]
3. Ay H, Arsava EM, Andsberg G, Benner T, Brown RD Jr., Chapman SN, Cole JW, Delavaran H, Dichgans M, Engstrom G, et al. Pathogenic ischemic stroke phenotypes in the NINDS-stroke genetics network. Stroke. 2014;45:3589–3596. doi: 10.1161/STROKEAHA.114.007362 [PubMed: 25378430]
4. Ay H Etiologic classification of ischemic stroke. Grotta, Albers, Broderick, Kasner, Lo, Mendelow, Sacco RL, Wong, eds. In: Stroke: Pathophysiology, Diagnosis, Management. Elsevier Inc.; 2015.
5. Rothwell PM, Eliasziw M, Gutnikov SA, Fox AJ, Taylor DW, Mayberg MR, Warlow CP, Barnett HJ, Carotid Endarterectomy Trialists C. Analysis of pooled data from the randomised controlled trials of endarterectomy for symptomatic carotid stenosis. Lancet. 2003;361:107–116. doi: 10.1016/s0140-6736(03)12228-3 [PubMed: 12531577]
6. Barnett HJ, Taylor DW, Eliasziw M, Fox AJ, Ferguson GG, Haynes RB, Rankin RN, Clagett GP, Hachinski VC, Sackett DL, et al. Benefit of carotid endarterectomy in patients with symptomatic moderate or severe stenosis. North American Symptomatic Carotid Endarterectomy Trial Collaborators. N Engl J Med. 1998;339:1415–1425. doi: 10.1056/NEJM199811123392002 [PubMed: 9811916]
7. Marquardt L, Geraghty OC, Mehta Z, Rothwell PM. Low risk of ipsilateral stroke in patients with asymptomatic carotid stenosis on best medical treatment: a prospective, population-based study. Stroke. 2010;41:e11–17. doi: 10.1161/STROKEAHA.109.561837 [PubMed: 19926843]
8. den Hartog AG, Achterberg S, Moll FL, Kappelle LJ, Visseren FL, van der Graaf Y, Algra A, de Borst GJ, Group SS. Asymptomatic carotid artery stenosis and the risk of ischemic stroke according to subtype in patients with clinical manifest arterial disease. Stroke. 2013;44:1002–1007. doi: 10.1161/STROKEAHA.111.669267 [PubMed: 23404720]
9. Saba L, Yuan C, Hatsukami TS, Balu N, Qiao Y, DeMarco JK, Saam T, Moody AR, Li D, Matouk CC, et al. Carotid Artery Wall Imaging: Perspective and Guidelines from the ASNR Vessel Wall Imaging Study Group and Expert Consensus Recommendations of the American Society of Neuroradiology. AJNR Am J Neuroradiol. 2018;39:E9–E31. doi: 10.3174/ajnr.A5488 [PubMed: 29326139]
10. Mullen MT, Jim J. Management of asymptomatic extracranial atherosclerotic disease. In: UpToDate, Kasner SE, Eidt JF, Mills JL Sr (Eds), UptoDate, Waltham, MA (Accessed on December 14, 2021).
11. Zhu G, Hom J, Li Y, Jiang B, Rodriguez F, Fleischmann D, Saloner D, Porcu M, Zhang Y, Saba L, et al. Carotid plaque imaging and the risk of atherosclerotic cardiovascular disease. Cardiovasc Diagn Ther. 2020;10:1048–1067. doi: 10.21037/cdt.2020.03.10 [PubMed: 32968660]
12. Fayad Z, Fuster V. Characterization of Atherosclerotic Plaques by Magnetic Resonance Imaging. Annals of the New York Academy of Sciences. 2000;902:173–186. doi: 10.1111/j.1749-6632.2000.tb06312.x [PubMed: 10865837]
13. Nighoghossian N, Derex L, Douek P. The vulnerable carotid artery plaque: current imaging methods and new perspectives. Stroke. 2005;36:2764–2772. doi: 10.1161/01.STR.0000190895.51934.43 [PubMed: 16282537]
14. Spagnoli LG, Mauriello A, Sangiorgi G, Fratoni S, Bonanno E, Schwartz RS, Piepgras DG, Pistolese R, Ippoliti A, Holmes DR Jr. Extracranial thrombotically active carotid plaque as a risk factor for ischemic stroke. JAMA. 2004;292:1845–1852. doi: 10.1001/jama.292.15.1845 [PubMed: 15494582]

15. Stein-Merlob AF, Hara T, McCarthy JR, Mauskapf A, Hamilton JA, Ntziachristos V, Libby P, Jaffer FA. Atheroma Susceptible to Thrombosis Exhibit Impaired Endothelial Permeability In Vivo as Assessed by Nanoparticle-Based Fluorescence Molecular Imaging. Circulation: Cardiovascular Imaging. 2017;10:2715–2719. doi: 10.1161/CIRCIMAGING.116.005813

16. Davies JR, Izquierdo-Garcia D, Rudd JHF, Figg N, Richards HK, Bird JLE, Aigbirhio FI, Davenport AP, Weissberg PL, Fryer TD, et al. FDG-PET can distinguish inflamed from non-inflamed plaque in an animal model of atherosclerosis. Int J Cardiovasc Imaging. 2010;26:41–48. doi: 10.1007/s10554-009-9506-6

17. Izquierdo-Garcia D, Davies JR, Graves MJ, Rudd JHF, Gillard JH, Weissberg PL, Fryer TD, Warburton EA. Comparison of methods for magnetic resonance-guided [18-F]fluorodeoxyglucose positron emission tomography in human carotid arteries: reproducibility, partial volume correction, and correlation between methods. Stroke; a journal of cerebral circulation. 2009;40:86–93. doi: 10.1161/STROKEAHA.108.521393

18. Tawakol A, Migrino RQ, Bashian GG, Bedri S, Vermylen D, Cury RC, Yates D, LaMuraglia GM, Furie K, Houser S, et al. In vivo 18F-Fluorodeoxyglucose positron emission tomography imaging provides a noninvasive measure of carotid plaque inflammation in patients. J Am Coll Cardiol. 2006;48:1818–1824. doi: [PubMed: 17084256]

19. Moore WS, Barnett HJ, Beebe HG, Bernstein EF, Brener BJ, Brott T, Caplan LR, Day A, Goldstone J, Hobson RW 2nd, et al. Guidelines for carotid endarterectomy. A multidisciplinary consensus statement from the Ad Hoc Committee, American Heart Association. Circulation. 1995;91:566–579. doi: 10.1161/01.cir.91.2.566 [PubMed: 7805271]

20. Mughal MM, Khan MK, DeMarco JK, Majid A, Shamoun F, Abela GS. Symptomatic and asymptomatic carotid artery plaque. Expert Rev Cardiovasc Ther. 2011;9:1315–1330. doi: 10.1586/erc.11.120 [PubMed: 21985544]

21. Fabiani I, Palombo C, Caramella D, Nilsson J, De Caterina R. Imaging of the vulnerable carotid plaque: Role of imaging techniques and a research agenda. Neurology. 2020;94:922–932. doi: 10.1212/WNL.0000000000009480 [PubMed: 32393647]

22. den Hartog AG, Bovens SM, Koning W, Hendrikse J, Luijten PR, Moll FL, Pasterkamp G, de Borst GJ. Current status of clinical magnetic resonance imaging for plaque characterisation in patients with carotid artery stenosis. Eur J Vasc Endovasc Surg. 2013;45:7–21. doi: 10.1016/j.ejvs.2012.10.022 [PubMed: 23200607]

23. Cai J, Hatsukami TS, Ferguson MS, Kerwin WS, Saam T, Chu B, Takaya N, Polissar NL, Yuan C. In vivo quantitative measurement of intact fibrous cap and lipid-rich necrotic core size in atherosclerotic carotid plaque: comparison of high-resolution, contrast-enhanced magnetic resonance imaging and histology. Circulation. 2005;112:3437–3444. doi: 10.1161/CIRCULATIONAHA.104.528174 [PubMed: 16301346]

24. Huibers A, de Borst GJ, Wan S, Kennedy F, Giannopoulos A, Moll FL, Richards T. Non-invasive Carotid Artery Imaging to Identify the Vulnerable Plaque: Current Status and Future Goals. Eur J Vasc Endovasc Surg. 2015;50:563–572. doi: 10.1016/j.ejvs.2015.06.113 [PubMed: 26298222]

25. Osborn EA, Jaffer FA. Advances in molecular imaging of atherosclerotic vascular disease. Curr Opin Cardiol. 2008;23:620–628. doi: 10.1097/HCO.0b013e328310fc7e [PubMed: 18830079]

26. Kooi ME, Cappendijk VC, Cleutjens KB, Kessels AG, Kitslaar PJ, Borgers M, Frederik PM, Daemen MJ, van Engelshoven JM. Accumulation of ultrasmall superparamagnetic particles of iron oxide in human atherosclerotic plaques can be detected by in vivo magnetic resonance imaging. Circulation. 2003;107:2453–2458. doi: 10.1161/01.CIR.0000068315.98705.CC [PubMed: 12719280]

27. Manca G, Parenti G, Bellina R, Boni G, Grosso M, Bernini W, Palombo C, Paterni M, Pelosi G, Lanza M, et al. 111In platelet scintigraphy for the noninvasive detection of carotid plaque thrombosis. Stroke. 2001;32:719–727. doi: 10.1161/01.str.32.3.719 [PubMed: 11239193]

28. Irkle A, Vesey AT, Lewis DY, Skepper JN, Bird JL, Dweck MR, Joshi FR, Gallagher FA, Warburton EA, Bennett MR, et al. Identifying active vascular microcalcification by (18)F-sodium fluoride positron emission tomography. Nat Commun. 2015;6:7495. doi: 10.1038/ncomms8495 [PubMed: 26151378]

29. Rudd JH, Warburton EA, Fryer TD, Jones HA, Clark JC, Antoun N, Johnstrom P, Davenport AP, Kirkpatrick PJ, Arch BN, et al. Imaging atherosclerotic plaque inflammation with

[18F]-fluorodeoxyglucose positron emission tomography. Circulation. 2002;105:2708–2711. doi: 10.1161/01.cir.0000020548.60110.76 [PubMed: 12057982]

30. Kietselaer BL, Reutelingsperger CP, Heidendal GA, Daemen MJ, Mess WH, Hofstra L, Narula J. Noninvasive detection of plaque instability with use of radiolabeled annexin A5 in patients with carotid-artery atherosclerosis. N Engl J Med. 2004;350:1472–1473. doi: 10.1056/NEJM200404013501425
31. Rudd JH, Myers KS, Bansilal S, Machac J, Rafique A, Farkouh M, Fuster V, Fayad ZA. (18)Fluorodeoxyglucose positron emission tomography imaging of atherosclerotic plaque inflammation is highly reproducible: implications for atherosclerosis therapy trials. J Am Coll Cardiol. 2007;50:892–896. doi: 10.1016/j.jacc.2007.05.024 [PubMed: 17719477]
32. Evans NR, Tarkin JM, Buscombe JR, Markus HS, Rudd JHF, Warburton EA. PET imaging of the neurovascular interface in cerebrovascular disease. Nat Rev Neurol. 2017;13:676–688. doi: 10.1038/nrneurol.2017.129 [PubMed: 28984315]
33. Kelly PJ, Camps-Renom P, Giannotti N, Marti-Fabregas J, Murphy S, McNulty J, Barry M, Barry P, Calvet D, Coutts SB, et al. Carotid Plaque Inflammation Imaged by (18)F-Fluorodeoxyglucose Positron Emission Tomography and Risk of Early Recurrent Stroke. Stroke. 2019;50:1766–1773. doi: 10.1161/STROKEAHA.119.025422 [PubMed: 31167623]
34. Kelly PJ, Camps-Renom P, Giannotti N, Marti-Fabregas J, McNulty JP, Baron JC, Barry M, Coutts SB, Cronin S, Delgado-Mederos R, et al. A Risk Score Including Carotid Plaque Inflammation and Stenosis Severity Improves Identification of Recurrent Stroke. Stroke. 2020;51:838–845. doi: 10.1161/STROKEAHA.119.027268 [PubMed: 31948355]
35. Jaffer FA, Libby P, Weissleder R. Molecular Imaging of Cardiovascular Disease. Circulation. 2007;116:1052–1061. doi: 10.1161/CIRCULATIONAHA.106.647164 [PubMed: 17724271]
36. Sanz J, Fayad ZA. Imaging of atherosclerotic cardiovascular disease. Nature. 2008;451:953–957. doi: [PubMed: 18288186]
37. Lindner JR. Molecular imaging of thrombus: technology in evolution. Circulation. 2012;125:3057–3059. doi: 10.1161/CIRCULATIONAHA.112.112672 [PubMed: 22647974]
38. Ciesienski KL, Caravan P. Molecular MRI of Thrombosis. Curr Cardiovasc Imaging Rep. 2010;4:77–84. doi: 10.1007/s12410-010-9061-5 [PubMed: 21253438]
39. Kolodziej AF, Nair SA, Graham P, McMurry TJ, Ladner RC, Wescott C, Sexton DJ, Caravan P. Fibrin specific peptides derived by phage display: characterization of peptides and conjugates for imaging. Bioconjug Chem. 2012;23:548–556. doi: 10.1021/bc200613e [PubMed: 22263840]
40. Hara T, Ughi GJ, McCarthy JR, Erdem SS, Mauskapf A, Lyon SC, Fard AM, Edelman ER, Tearney GJ, Jaffer FA. Intravascular fibrin molecular imaging improves the detection of unhealed stents assessed by optical coherence tomography in vivo. Eur Heart J. 2017;38:447–455. doi: 10.1093/eurheartj/ehv677 [PubMed: 26685129]
41. Uppal R, Ciesienski KL, Chonde DB, Loving GS, Caravan P. Discrete bimodal probes for thrombus imaging. J Am Chem Soc. 2012;134:10799–10802. doi: 10.1021/ja3045635 [PubMed: 22698259]
42. Ciesienski KL, Yang Y, Ay I, Chonde DB, Loving GS, Rietz Ta, Catana C, Caravan P. Fibrin-targeted PET probes for the detection of thrombi. Mol Pharm. 2013;10:1100–1110. doi: 10.1021/mp300610s [PubMed: 23327109]
43. Ay I, Blasi F, Rietz TA, Rotile NJ, Kura S, Brownell AL, Day H, Oliveira BL, Looby RJ, Caravan P. In vivo molecular imaging of thrombosis and thrombolysis using a fibrin-binding positron emission tomographic probe. Circ Cardiovasc Imaging. 2014;7:697–705. doi: 10.1161/CIRCIMAGING.113.001806 [PubMed: 24777937]
44. Blasi F, Oliveira BL, Rietz TA, Rotile NJ, Naha PC, Cormode DP, Izquierdo-Garcia D, Catana C, Caravan P. Multisite Thrombus Imaging and Fibrin Content Estimation With a Single Whole-Body PET Scan in Rats. Arteriosclerosis, thrombosis, and vascular biology. 2015;35:2114–2121. doi: 10.1161/ATVBAHA.115.306055
45. Uppal R, Catana C, Ay I, Benner T, Sorensen AG, Caravan P. Bimodal thrombus imaging: simultaneous PET/MR imaging with a fibrin-targeted dual PET/MR probe--feasibility study in rat model. Radiology. 2011;258:812–820. doi: 10.1148/radiol.10100881 [PubMed: 21177389]

46. Izquierdo-Garcia D, Désogère P, Philip AL, Mekkaoui C, Weiner RB, Catalano OA, Iris Chen Y-C, DeFaria Yeh D, Mansour M, Catana C, et al. Detection and Characterization of Thrombosis in Humans Using Fibrin-Targeted Positron Emission Tomography and Magnetic Resonance. JACC: Cardiovascular Imaging. 2021. doi: 10.1016/j.jcmg.2021.08.009
47. Bošnjaković V, Janković B, Horvat J, Čvoric J. RADIOLABELLED ANTI-HUMAN FIBRIN ANTIBODY: A NEW THROMBUS-DETECTING AGENT. The Lancet. 1977;309:452–454. doi: 10.1016/S0140-6736(77)91944-4
48. Macfarlane D, Socrates A, Eisenberg P, Larcos G, Roach P, Gerometta M, Smart R, Tsui W, Scott AM. Imaging of deep venous thrombosis in patients using a radiolabelled anti-D-dimer Fab' fragment (99mTc-DI-DD3B6/22–80B3): results of a phase I trial. Eur J Nucl Med Mol Imaging. 2009;36:250–259. doi: [PubMed: 18800218]
49. Lanza GM, Cui G, Schmieder AH, Zhang H, Allen JS, Scott MJ, Williams T, Yang X. An unmet clinical need: The history of thrombus imaging. Journal of Nuclear Cardiology. 2019;26:986–997. doi: 10.1007/s12350-017-0942-8 [PubMed: 28608182]
50. Elhfnawy AM, Volkmann J, Schliesser M, Fluri F. Symptomatic vs. Asymptomatic 20–40% Internal Carotid Artery Stenosis: Does the Plaque Size Matter? Frontiers in Neurology. 2019;10:1–7. doi: 10.3389/fneur.2019.00960 [PubMed: 30761061]
51. Hoffman EJ, Huang SC, Phelps ME. Quantitation in positron emission computed tomography: 1. Effect of object size. J Comput Assist Tomogr. 1979;3:299–308. doi: [PubMed: 438372]
52. Chen YC, Bui AV, Diesch J, Manasseh R, Hausding C, Rivera J, Haviv I, Agrotis A, Htun NM, Jowett J, et al. A novel mouse model of atherosclerotic plaque instability for drug testing and mechanistic/therapeutic discoveries using gene and microRNA expression profiling. Circ Res. 2013;113:252–265. doi: 10.1161/CIRCRESAHA.113.301562 [PubMed: 23748430]
53. Cheng C, Tempel D, van Haperen R, van der Baan A, Grosveld F, Daemen MJ, Krams R, de Crom R. Atherosclerotic lesion size and vulnerability are determined by patterns of fluid shear stress. Circulation. 2006;113:2744–2753. doi: 10.1161/CIRCULATIONAHA.105.590018 [PubMed: 16754802]
54. Carstairs KC. The identification of platelets and platelet antigens in histological sections. The Journal of Pathology and Bacteriology. 1965;90:225–231 [PubMed: 5320852]

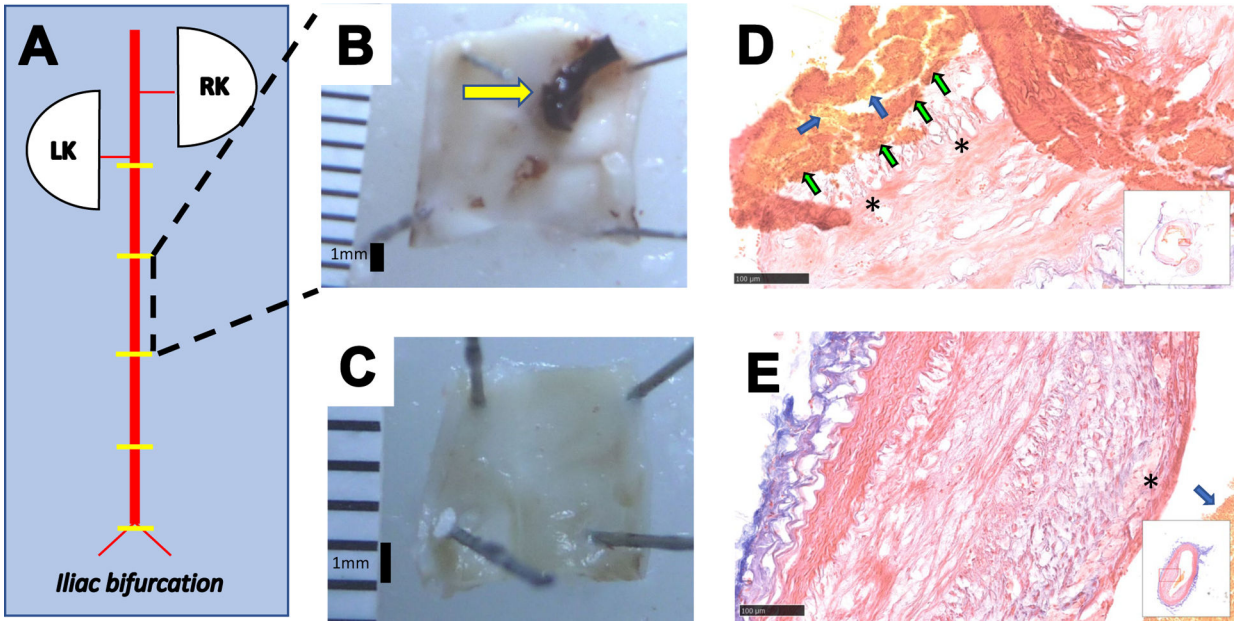

Figure 1.

Pharmacological triggering induces plaque disruption in the rabbit model of atherosclerosis. (A): Schematic of the abdominal aorta (AA) from the renal to the iliac bifurcations. Yellow lines represent the approximate location of the segments for histopathology. Plaque disruption was diagnosed by identification of thrombus in the AA on gross pathology and Carstairs'-stained sections. Representative post-mortem AA photographs from a rabbit with successful plaque rupture showing intraluminal thrombus attached to the vessel wall (yellow arrow in B) vs. a control atherosclerosis-bearing rabbit (C) showing a clear luminal surface with plaque but without thrombosis. Representative light microscopy images of Carstairs' staining of the rabbit AA from rabbits with (D) and without (E) plaque rupture. In rabbits demonstrating plaque disruption(D), the fibrous cap of the plaque (marked by stars) was broken, and the thrombus containing yellow-stained area suggesting the presence of erythrocytes (blue arrows) and bright red-stained fibrin (green arrows) were visible. In the non-disrupted aorta (E), the fibrous cap (marked by a star) was intact, and even though yellow-stained area suggesting the erythrocytes were visible (blue arrow) since the tissue was not perfused, there were neither fibrin nor a thrombus. RK: right kidney, LK: left kidney.

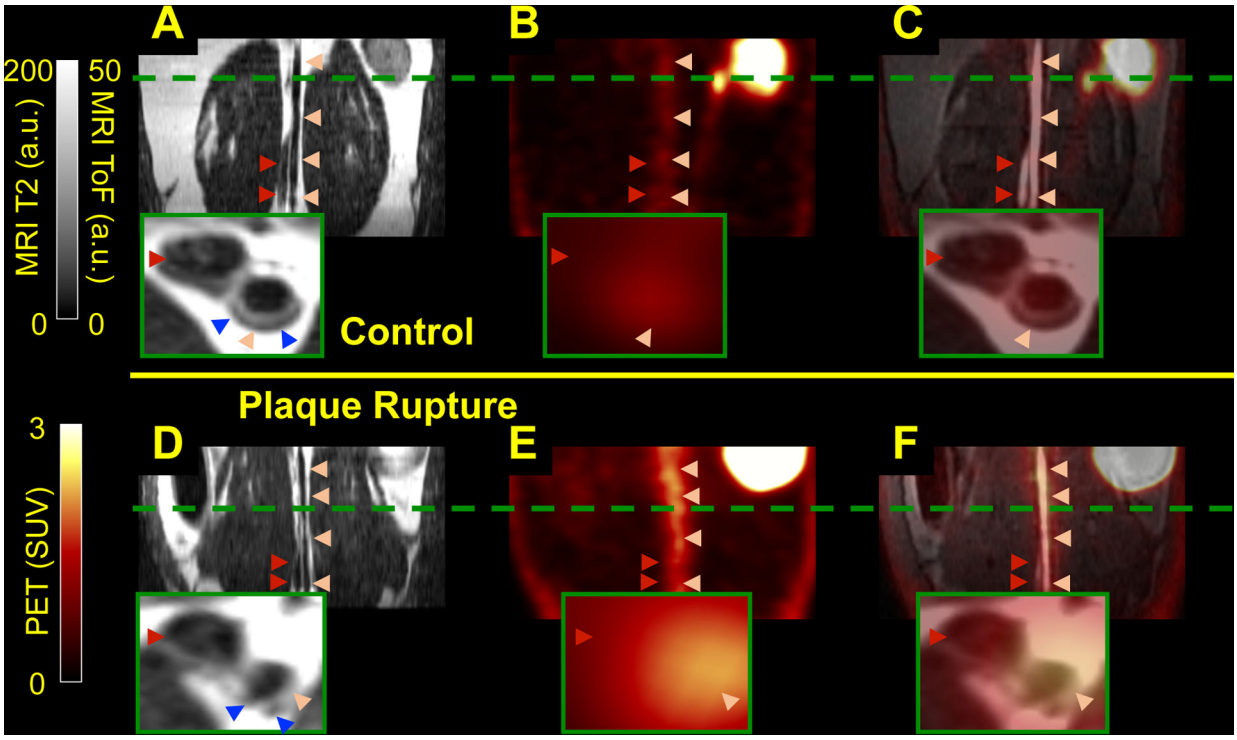

Figure 2:

Fibrin-binding probe uptake increases in rabbits with plaque disruption. Representative in vivo PET/MR images from atherosclerotic rabbits show increased uptake of PET probe on animals with (D-F) vs. without (A-C) plaque rupture: Dark-blood T2-weighted (A, D), PET images (B, E), showed patchy fibrin signal along the AA in rabbits with plaque disruption; and fused PET/MR images with ToF (C and F). Light pink arrowheads point to the AA; dark red arrowheads point to the inferior vena cava. Green dashed lines to locate the axial close-up images (insert) that show the atherosclerotic plaques as light gray areas (blue arrowheads in A and D): smooth plaques for the non-ruptured vs. non-smooth for the triggered animals. a.u.: arbitrary units.

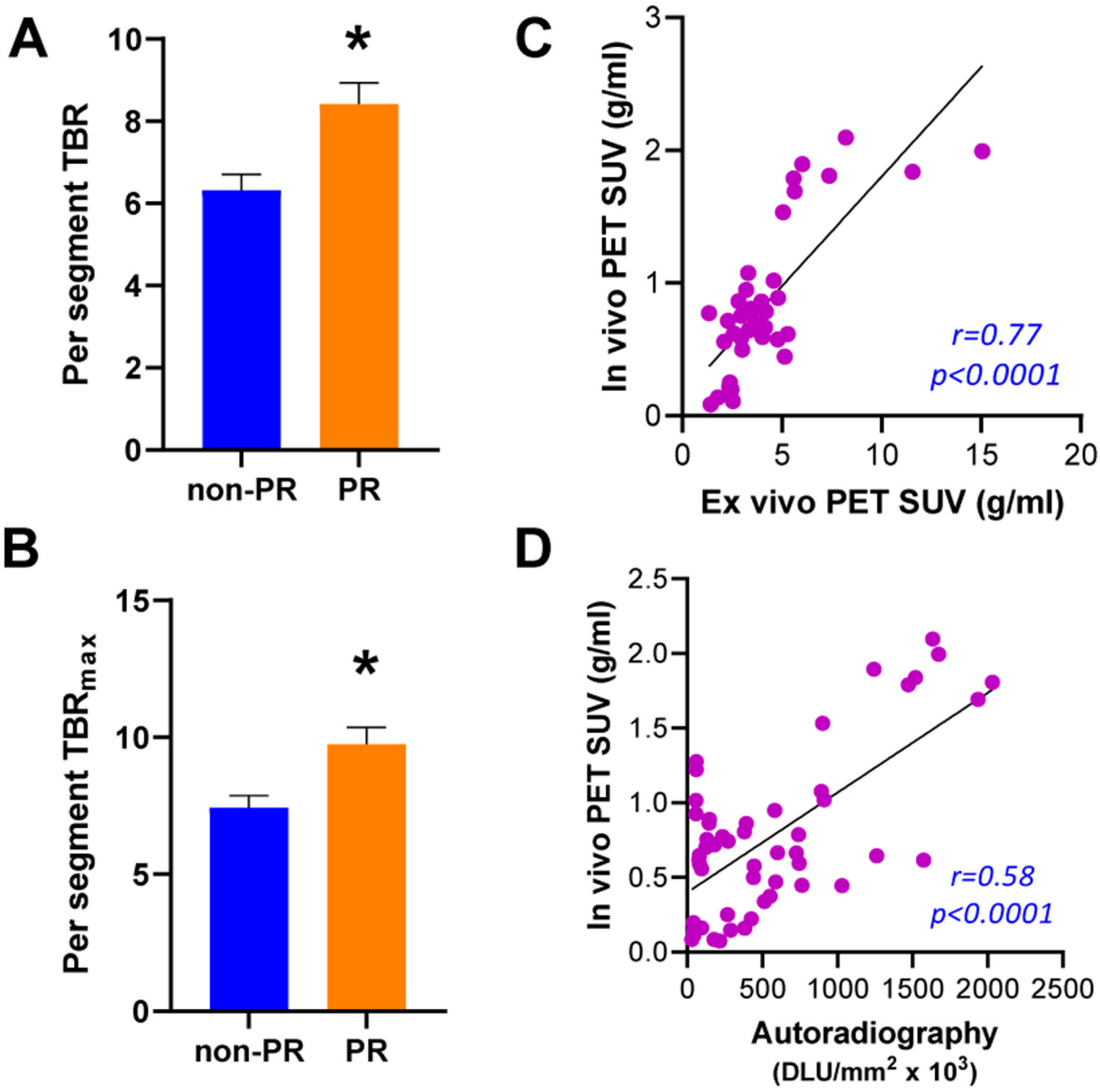

Figure 3:

Segmental analysis of the in vivo PET results and correlation between in vivo and the ex vivo data. Per-segment analyses of TBR (A) and TBR_{max} (B) revealed significant aortic uptake differences between plaque rupture vs. non-ruptured. Correlation plots for in vivo vs. ex vivo PET (Pearson's, C) and in vivo vs. autoradiography (Spearman's, D) for the per-segment analysis. DLU: digital light units.

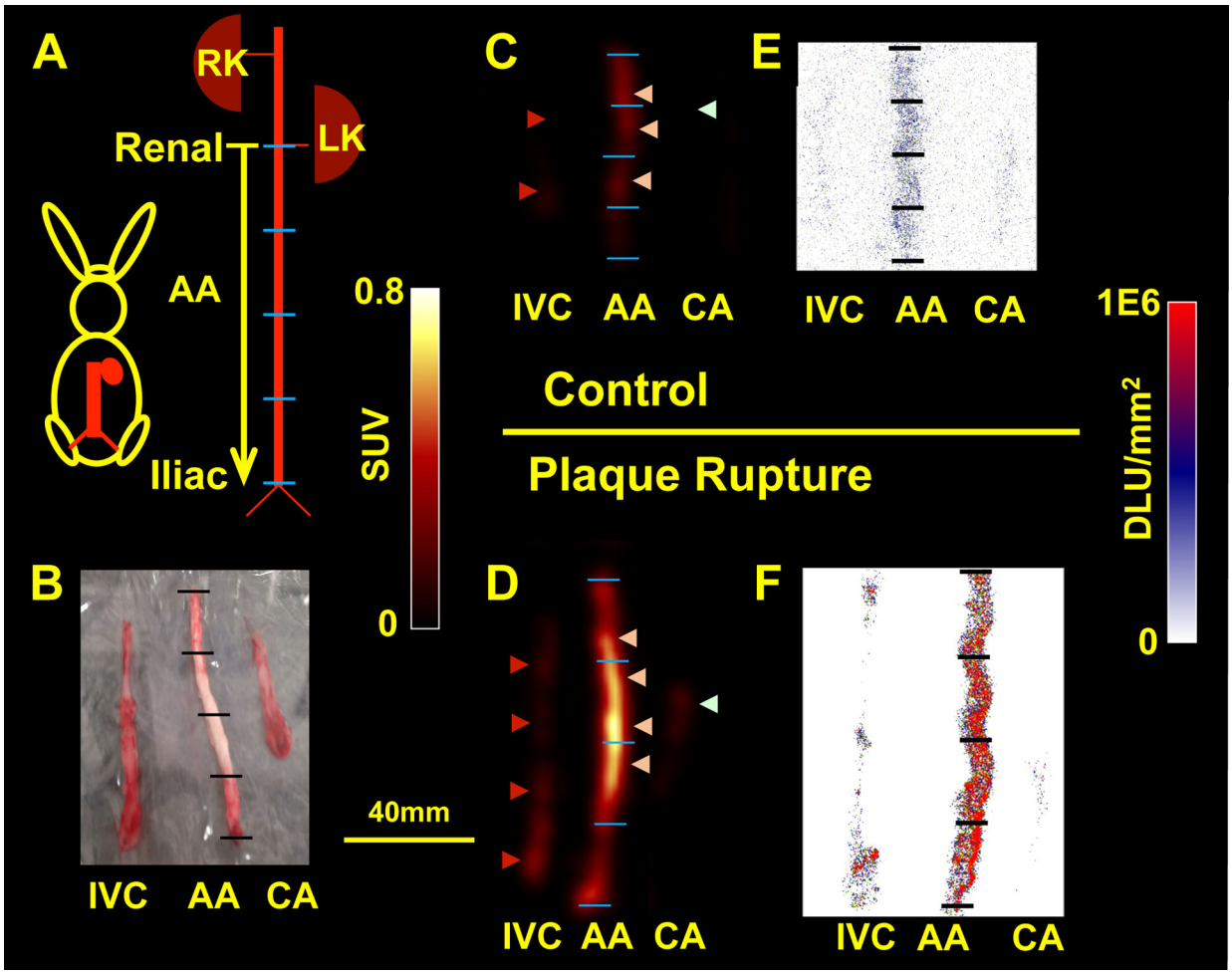

Figure 4:

Ex vivo PET imaging and autoradiography confirmed in vivo PET/MRI results: (A) Schematic of the excised AA (segment from the renal to iliac bifurcations). (B) Picture of samples ready for ex vivo PET imaging (CA: carotid artery, IVC: inferior vena cava). Ex vivo (C-D) and autoradiography (E-F) images of a non-plaque thrombosis segment (C and E) vs. plaque thrombosis segment (D and F) showing focal increases in ^{68}Ga-CM246 uptake along the AA in animals with rupture compared with the IVC or non-plaque rupture rabbit. Light pink arrowheads point to the AA. Dark red arrowheads point to the IVC, and light green arrowheads point to the CA. Length bar (B-F) = 40mm. DLU: digital light units. RK: right kidney, LK: left kidney.

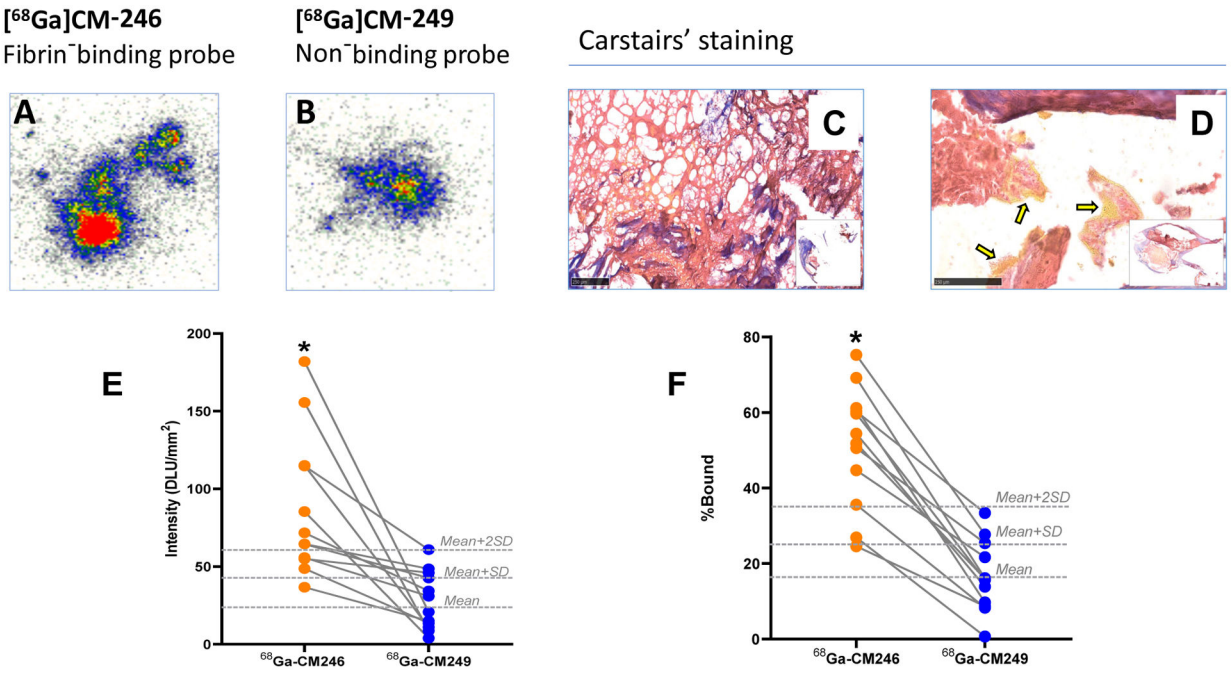

Figure 5:

Uptake of the fibrin-binding probe ^{68}Ga-CM246 was significantly higher than the non-binding control probe in specimens from carotid endarterectomy patients. Representative autoradiography (A-B) and light microscopy images of Carstairs' stained sections (C-D) from patient specimens with high ^{68}Ga-CM246 uptake, displaying an intense presence of fibrin (red-stained areas) with or without accompanying yellow areas that suggest the presence of erythrocytes (yellow arrows in panel D). In addition, fibrin meshes were observable in some high-uptake specimens (C). Autoradiography (E) and functional probe assay (F) of specimens from all patients revealed a variable but significantly increased ($P<0.05$) uptake of fibrin-binding probe ^{68}Ga-CM246 compared to non-binding probe ^{68}Ga-CM249. Dashed lines: ^{68}Ga-CM249 Mean, Mean + SD, and Mean + 2SD cutoff lines. DLU: digital light units.

Table 1:

Summary of ROC analysis using gross pathology as the gold standard. Threshold = interval of values that achieve the highest accuracy.

	Per-animal	Per-segment
TBR	Threshold = [6.7 – 7.6]	Threshold = [7.0]
	Sensitivity = 71%	Sensitivity = 82%
	Specificity = 83%	Specificity = 67%
	Accuracy = 77%	Accuracy = 73%
TBR_{max}	Threshold = [6.9 – 7.5]	Threshold = [7.7 – 8.0]
	Sensitivity = 100%	Sensitivity = 82%
	Specificity = 67%	Specificity = 63%
	Accuracy = 85%	Accuracy = 71%